PAPER

Flexural bending to approximate cortical forces exerted by electrocorticography (ECoG) arrays

To cite this article: Nicholas S Witham *et al* 2022 *J. Neural Eng.* **19** 046041

View the article online for updates and enhancements.

Journal of Neural Engineering

PAPER

Flexural bending to approximate cortical forces exerted by electrocorticography (ECoG) arrays

Nicholas S Witham[1] ⓘ, Christopher F Reiche[1] ⓘ, Thomas Odell[1] ⓘ, Katrina Barth[2] ⓘ, Chia-Han Chiang[2] ⓘ, Charles Wang[2] ⓘ, Agrita Dubey[3], Katie Wingel[3], Sasha Devore[3] ⓘ, Daniel Friedman[3] ⓘ, Bijan Pesaran[4] ⓘ, Jonathan Viventi[2] ⓘ and Florian Solzbacher[1,*] ⓘ

[1] The University of Utah, Salt Lake City, UT, United States of America
[2] Duke University, Durham, NC, United States of America
[3] New York University Grossman School of Medicine, New York City, NY, United States of America
[4] New York University, New York City, NY, United States of America
* Author to whom any correspondence should be addressed.

E-mail: florian.solzbacher@utah.edu

Abstract

Objective. The force that an electrocorticography (ECoG) array exerts on the brain manifests when it bends to match the curvature of the skull and cerebral cortex. This force can negatively impact both short-term and long-term patient outcomes. Here we provide a mechanical characterization of a novel liquid crystal polymer (LCP) ECoG array prototype to demonstrate that its thinner geometry reduces the force potentially applied to the cortex of the brain. *Approach.* We built a low-force flexural testing machine to measure ECoG array bending forces, calculate their effective flexural moduli, and approximate the maximum force they could exerted on the human brain. *Main results.* The LCP ECoG prototype was found to have a maximal force less than 20% that of any commercially available ECoG arrays that were tested. However, as a material, LCP was measured to be as much as $24\times$ more rigid than silicone, which is traditionally used in ECoG arrays. This suggests that the lower maximal force resulted from the prototype's thinner profile ($2.9\times$–$3.25\times$). *Significance.* While decreasing material stiffness can lower the force an ECoG array exhibits, our LCP ECoG array prototype demonstrated that flexible circuit manufacturing techniques can also lower these forces by decreasing ECoG array thickness. Flexural tests of ECoG arrays are necessary to accurately assess these forces, as material properties for polymers and laminates are often scale dependent. As the polymers used are anisotropic, elastic modulus cannot be used to predict ECoG flexural behavior. Accounting for these factors, we used our four-point flexure testing procedure to quantify the forces exerted on the brain by ECoG array bending. With this experimental method, ECoG arrays can be designed to minimize force exerted on the brain, potentially improving both acute and chronic clinical utility.

1. Introduction

A subdural electrocorticography (ECoG) array is a grid of neuroelectrodes that is used to monitor brain activity [1–4]. Clinically, ECoG is used to determine the origins of epileptiform activity, map functional regions of the brain, and monitor brain function during neurosurgery. ECoG is also used to research cognitive brain functions, and is particularly valuable for studies of uniquely human brain functions that cannot be directly studied in animals, such as those supporting speech and language [5–8]. The signal quality and resolution of ECoG arrays is much higher than conventional extracranial electroencephalography and reflects the activity of neurons recorded nearby the electrode [9]. However, ECoG placement requires invasive procedures, involving a craniotomy, where a portion of the skull is removed,
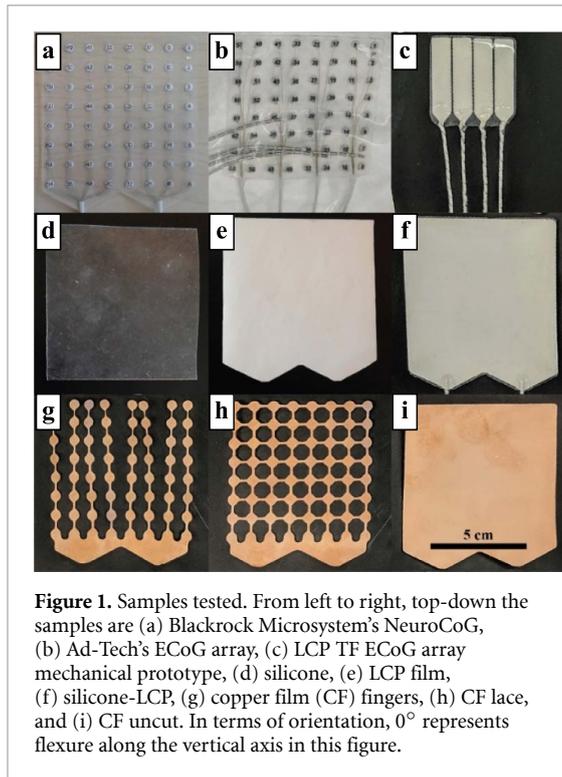
Figure 1. Samples tested. From left to right, top-down the samples are (a) Blackrock Microsystem's NeuroCoG, (b) Ad-Tech's ECoG array, (c) LCP TF ECoG array mechanical prototype, (d) silicone, (e) LCP film, (f) silicone-LCP, (g) copper film (CF) fingers, (h) CF lace, and (i) CF uncut. In terms of orientation, 0° represents flexure along the vertical axis in this figure.

and a durotomy, where the dura mater is resected to give access to the cortical surface [10, 11].

In addition to the surgical risks that come with a craniotomy and durotomy, placing an ECoG array on the brain, such as those seen in figure 1, exerts a force on the brain due to the array's bending stiffness [1, 12–16]. Previous work has shown that increasing pressure (force divided by contact area) on neurons beyond 0.1 MPa has short-term effects that can manifest within a fraction of a second to as much as 2 h after a stimulus, depending on its duration and frequency. This pressure increase is correlated with decreased action potential amplitude and conduction velocity [17, 18]. If the pressure is too large, then immediate cellular damage can also occur [19]. Smaller increases in brain pressure can also lead to cortical cell death, as intracranial pressure must be less than systemic blood pressure for nutrients to diffuse from blood [20]. For example, in the Cushing response, the brain stem experiences hypoxia because the cerebral perfusion pressure drops below 15 mmHg (2.00 kPa). To compensate, the body raises blood pressure and decreases pulse rate. If left untreated, this can lead to brain ischemia, herniation, or hemorrhage [17, 19]. While increased localized pressure is less dire than systemic intracranial pressure changes, these effects are still present, and headaches and other short-term changes in patient comfort can manifest soon after placement of less flexible ECoG arrays. Furthermore, local pressure may lead to stasis in cortical veins leading to thrombosis, edema and hemorrhage [21, 22]. The effects can be characterized from the measurement of midline shift on post-operative CT/MRI scans [23].

In addition to persistent short-term effects, long-term issues relating to the placement of ECoG arrays can also manifest days or weeks after the implantation surgery. Previous work has shown that a long-term foreign body response within the central nervous system is triggered by devices exerting a pressure greater than 100 Pa [24]. Due to this phenomenon, as well as the risks associated with neurosurgery, many modern devices have been designed with flexible components to decrease the risk of longer-term interaction with the nervous system and brain tissue [25, 26].

To create a chronically implantable ECoG array that conforms to the gyri of the brain with fewer adverse effects, a highly flexible liquid crystal polymer (LCP) thin-film (TF) ECoG array mechanical prototype was designed and produced (figure 1(c)). The novel LCP ECoG array was composed of an LCP-TF circuit molded in silicone to create a low-profile, highly flexible device [16, 27–30]. LCP is an optimal material for flexible ECoG arrays. LCP has water permeability <25× that of polyimide, another commonly used TF substrate [31], and *in vitro* accelerated aging tests have demonstrated an implantable lifetime of >5 years at body temperature [16]. Lithographic patterning of metal layers on the LCP substrate enables the design of micro-ECoG (μECoG) arrays, thus greatly increasing the resolution of neural recordings in comparison to current clinical standard devices. LCP μECoG arrays have been used to record in animal and human subjects to acquire fine details of the spatial dynamics of cortical activity [30].

Because all final devices will have gold traces that are only 3–8 μm thick and 20 μm wide, it was assumed that the contribution of these traces to flexural bending force would be insignificant compared to the LCP [32]. The LCP and silicone phases together are 5× to 70× thicker than the wire traces and are more than 99% of the bulk volume. Therefore, the mechanical prototype was tested without metal traces, due to the anticipated minimal impact on mechanical stiffness. To quantitatively validate the efficacy of this ECoG device and others, we constructed a custom low-force material testing machine along with a corresponding evaluation procedure to conduct our four point flexural bending tests [12, 13, 33–35].

With our custom-made setup, we performed a four-point flexural bending test on our mechanical prototype (LCP-TF), two United States Food and Drug Administration (FDA) approved ECoG arrays, copper film (CF) laminated LCP made by Dyconex cut in different patterns, and samples of LCP and silicone (figure 1). The two FDA approved devices tested are Blackrock Microsystems' NeuroCoG [36, 37] and Ad-Tech's (FG64C-SP10X-000) [38, 39]; they both utilize a silicone substrate and have 64 evenly distributed electrodes in an 8 × 8 pattern. These devices will be referenced as Blackrock and Ad-Tech from this point forward.

To evaluate orientation specific response, each sample was tested at three different orientations (0°, 45°, and 90°). The convention of these orientations indicates the rotation of bending axis in respect to the vertical axis in figure 1 (i.e. 0° means bending along the vertical axis). Both LCP and silicone samples were tested by themselves to determine the individual contributions of the proposed materials. To test the maximum impact of selective pattern excision, we cut different patterns into the CF samples to determine how different patterns could affect the flexural bending force.

2. Methods

2.1. Mechanical testing setup design, construction, and function

We constructed our mechanical bend testing setup using mechanical components from Robotzone LLC (ServoCity®), a National Instruments https://blackrockneurotech.com/research/neuroscience-research-products/low-noise-ephys-electrodes/blackrock-electrode-concepts/ myDAQ data acquisition system (DAQ), an INA122 instrumentation amplifier, and MLT1030/d force sensor from ADInstruments Dunedin, New Zealand (figure 2). These components allowed for the construction of an assembly that could measure with high accuracy the force that an array configuration material generates under flexion.

The maximum myDAQ analogue input is 10 V [40] and the maximum force sensor output is 150 mV [41–44]. To prevent a voltage pull down or up by DAQ's analogue voltage measurement and to remove common mode noise, we used an instrumentation amplifier. In order to maximize the force resolution without saturation, a 4 kΩ resistor was used to set a gain (G) of 55 across the instrumentation amplifier.

As the motor turns the lead screw, the drive nut lowers the loading assembly. Once the loading rods contact the sample, they transmit force vertically to the stainless-steel cantilever blade(s). The force sensor uses these cantilever blade(s) to amplify the force transmitted to two silicon semiconductor strain gauges (top and bottom), which are connected in a Wheatstone bridge configuration. This creates a substantial electric signal for small forces. The myDAQ's analogue input resolution is 0.1 mV [40] and with one blade the force sensor's data sheet indicates that it outputs 9 mV gf^{-1} [41], so the force resolution of the system (with a gain of 55) was predicted to be 0.202 mg$_f$ or 1.98 μN.

With the motor's maximum speed of 105 RPM, the worm gear's ratio of 1:27, and the 1.33 mm pitch of the drive screw, the maximum speed of actuation is 5.17 mm min^{-1}. We considered this slow rate to be quasistatic loading for soft tissues such as the brain and is representative of strain rates seen during ECoG array positioning and use.
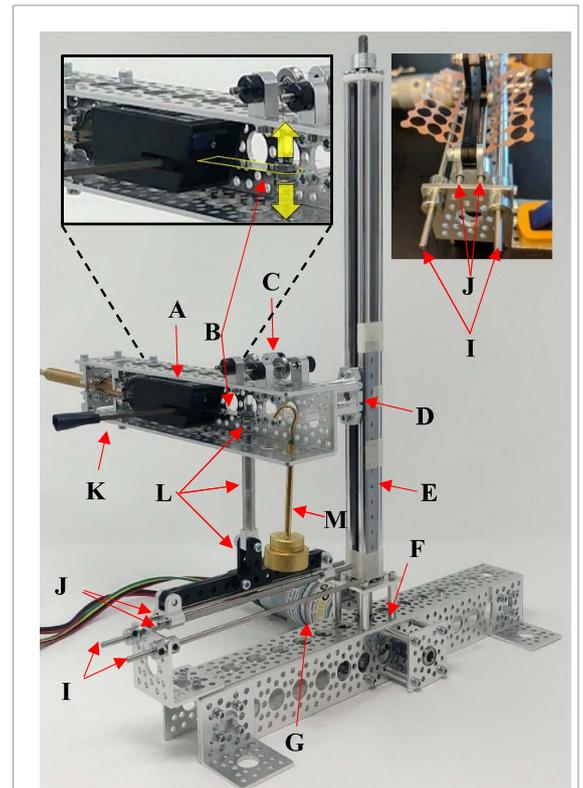

Figure 2. Low-force material testing machine. Machine can be varied in construction to accommodate various types of low force material tests. Key components are as follows: force sensor (A), cantilever blade (B), pulley system (C), lead screw actuator (D), metric ruler (E), worm gear (F), DC motor (G), 90° aluminum mounting brackets (H), support rods (I), loading rods (J), additional blades (K), loading assembly (L), and counterbalance (M). The inset in the top left depicts the cantilever blade's (B) deflection that is used to amplify forces on the sensor. The inset in the top right depicts the four-point flexural bending test of the CF lace sample in the 0° orientation.

The machine was calibrated by changing the mass of the counterbalance in 5 g increments ranging from 35 g to 95 g. At each unique mass, the deflection of the cantilever blade was measured with a pair of EZCal calipers and the DAQ recorded the voltage. Known stainless steel rod diameters and lengths ranging from 0.01 mm to 100 mm were used to evaluate the accuracy of the calipers with no notable errors. The results of this calibration can be found in the supplementary information. Once calibrated, the loading assembly was counterbalanced with a mass of 65 g. This produced the same deflection and voltage as the unweighted cantilever blade.

2.2. Sample fabrication

In addition to the two FDA-approved clinical devices (figures 1(a) and (b)), we tested seven different custom prototypes to characterize the flexural properties of various designs and combinations of LCP, copper foil, and silicone. All silicone was prepared in a 1:10 ratio of curing agent to elastomer base using the MDX4-4210 product from Dow Corning, a USP Class VI material. Adhesion was ensured

between LCP and silicone using Nusil Technologies MED1-161 silicone primer, a USP Class VI material which has passed ISO 10993-5 cytotoxicity testing. LCP samples were cut using a Silhouette Curio paper cutting machine to create various 2D patterns. Silicone molding was achieved using custom milled metal stencils. We tested a mechanical prototype of the novel LCP ECoG array which included four 9×40 mm strips of 50 μm thick LCP molded together with silicone to a total thickness of 200 μm (figure 1(c)). While no metal traces or contacts are included in this prototype, the LCP and silicone comprise the bulk of material in this device and therefore are the focus of mechanical testing, as justified in the introduction. We also tested a sheet of 600 μm thick silicone (figure 1(d)), a sheet of 50 μm thick LCP film (figure 1(e)), and a combined uniform sheet of LCP and silicone molded together to a total thickness of 410 μm (figure 1(f)). CF-laminated LCP sheets of 60 μm total thickness were cut in various patterns, all of which could accommodate an arrangement of contacts and wiring to match the silicone FDA approved clinical devices (figures 1(g)–(i)). Additional details regarding LCP device fabrication and design can be found in Chiang *et al* [30].

2.3. Flexural testing

Using calipers, all samples were physically measured in width, length, and thickness 12 times. The residual mass of the loading assembly was then digitally tared by the LabView VI, so that the sensor read 0.0000 g$_f$. To tare, the program recorded the baseline reading 2500 times at a 0.6 Hz sampling frequency.

Once tared, the sample was positioned horizontally along two stainless steel round support rods that were 26.94 mm apart. The two stainless steel loading rods (9.78 mm apart) were lowered 2 mm to nearly contact the sample. If gravity caused the sample to warp, the force sensor would output a non-zero reading and horizontal support would then be added next to the support rods to prevent premature flexure of the sample. The loading assembly was then lowered an additional 5 mm to flex the sample. Note that for this method to yield accurate data the materials measured must have linear mechanical behavior.

Once the sensor's output was recorded, the loading rods were raised by 7 mm, so the sample could be rotated or removed. The program reduces measurement noise by outputting a running average of the last 25 sensor measurements. To control for distance measurement errors generated by the Hall effect relative quadrature encoder, all displacement measurements were additionally verified with a 90° aluminum bracket and metric ruler fixed to the measurement assembly.

2.4. Data analysis

Based on the force measured by the sensor (F_{meas}) equations (1)–(6) are used to derive flexural modulus
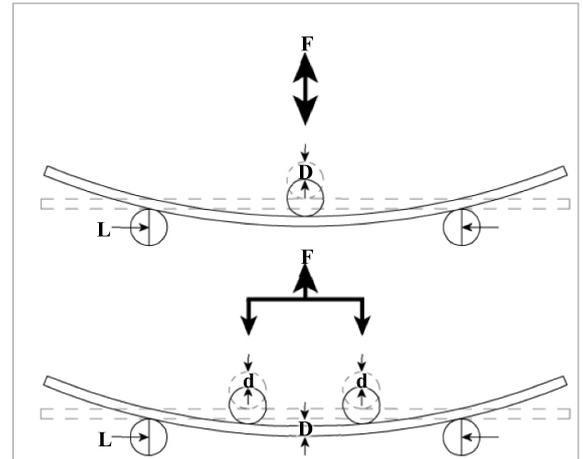

Figure 3. Three point and four point flexural bending tests. The sample is placed across two support rods and loading rod(s) that displace (d) to cause the sample to bend in a radius (r); deflecting its center (D). The sample exerts a force (F) upwards proportional to sample height (h), sample width (w), and gap span (L). Height, width, and radius are unlabeled. Please note that the shown bending, position, and orientation of the samples is valid for the mechanical testing only. During surgeries the bending amplitude, position and orientation of the samples is different.

(E_f) from the following variables: known mass (g), displacement of lead nut (z), sample height (h), cantilever deflection (k), displacement of loading rods (d), radius of curvature (r), sample width (w), gap span (L), tested deflection (D_t), force measured by sensor ($F_{measured}$), and true force experienced by sensor (F_{real}) [33–35, 44, 45]. These variables are illustrated in figure 3. These equations are based on the assumptions that (a) the loading rods are spaced apart by 1/3rd the distance of the gap span, (b) the flexure assembly bends the sample in a constant radius of curvature, and (c) the change in L is negligible,

$$F_{real} = (F_{meas} + 0.432)/0.220 \qquad (1)$$

$$k = 0.140 * F_{real} - 0.292 \qquad (2)$$

$$d = z + h - k \qquad (3)$$

$$r = \sqrt{\frac{L^2}{4} + \left(\frac{d}{2} - \frac{L^2}{9d}\right)^2} \qquad (4)$$

$$D_t = r - \sqrt{r^2 - \frac{L^2}{4}} \qquad (5)$$

$$E_f = 0.21 \frac{L^3 F}{w h^3 D_t}. \qquad (6)$$

The maximum force on the brain was calculated assuming a worst-case scenario, where the skull acts as two support points, and a single gyrus of the brain acts as the only loading point or bending fulcrum. Equation (7) below, utilizes the relationships of variables used in a three-point flexural bending test equation to determine the force that would be exerted

Table 1. ECoG array flexural test values at 0° orientation.

Sample (thickness)	Total force (mN)	Sample deflection (mm)	Flexural modulus (GPa)	Max force (mN)
CF uncut (60 μm)	$410 \pm 30^r \pm 0.02^s$	$0.59 \pm 0.5^r \pm 0.3^s$	$150 \pm 100^r \pm 100^s$	$880 \pm 700^r \pm 400^s$
CF lace (60 μm)	$250 \pm 40^r \pm 0.02^s$	$2.1 \pm 0.6^r \pm 0.3^s$	$27 \pm 10^r \pm 10^s$	$150 \pm 60^r \pm 20^s$
CF fingers (60 μm)	$64 \pm 9^r \pm 0.02^s$	$4.9 \pm 0.1^r \pm 0.3^s$	$2.9 \pm 0.5^r \pm 0.9^s$	$16 \pm 3^r \pm 0.9^s$
LCP film (40 μm)	$25 \pm 3^r \pm 0.02^s$	$5.5 \pm 0.05^r \pm 0.3^s$	$3.4 \pm 0.5^r \pm 1^s$	$5.7 \pm 0.8^r \pm 0.3^s$
LCP TF (200 μm)	$55 \pm 10^r \pm 0.02^s$	$5.2 \pm 0.2^r \pm 0.3^s$	$0.11 \pm 0.03^r \pm 0.01^s$	$13 \pm 4^r \pm 0.7^s$
Silicone (600 μm)	$180 \pm 20^r \pm 0.02^s$	$3.8 \pm 0.3^r \pm 0.3^s$	$0.011 \pm 0.002^r \pm 0.001^s$	$58 \pm 10^r \pm 4^s$
LCP & Silicone (410 μm)	$120 \pm 20^r \pm 0.02^s$	$4.4 \pm 0.3^r \pm 0.3^s$	$0.019 \pm 0.005^r \pm 0.002^s$	$35 \pm 9^r \pm 2^s$
Ad-Tech (850 μm)	$200 \pm 50^r \pm 0.02^s$	$3.6 \pm 0.7^r \pm 0.3^s$	$0.0047 \pm 0.002^r \pm 0.0004^s$	$70 \pm 30^r \pm 5^s$
Blackrock (580 μm)	$230 \pm 20^r \pm 0.02^s$	$2.8 \pm 0.3^r \pm 0.3^s$	$0.019 \pm 0.003^r \pm 0.002^s$	$100 \pm 20^r \pm 10^s$

r = random error.

s = systematic error.

if only one gyrus contacted the array if it was maximally flexed (D_m). D_m is equal to 1.5 mm as this flexion bends the sample, so that it is radius is 60 mm. This radius was determined to be the smallest of any cortex of an MRI brain-scan of a Caucasian female 38 years of age. This brain scan was obtained from the NIH 3D Print Exchange as an STL file (Model 3DPX-000320). Radius measurements were made in SOLIDWORKS by making an arch through three points on the same plane.

$$F_{max} = \frac{4E_f w h^3 D_m}{L^3} \qquad (7)$$

Gaussian error approximation was used to determine the bounds of uncertainty [46].

3. Results

3.1. Physical measurement and bending force
To utilize equations (1)–(5), we needed to measure the dimensions of samples: thickness (h), width (w), and length (l). The copper foil laminated LCP samples, LCP film, and silicone-LCP were cut to have the same surface area dimensions at 89.30 mm × 86.00 mm ($w \times l$). Respectively, the measured thicknesses were 0.06 mm, 0.04 mm, and 0.85 mm. These were similar in dimension to the Blackrock device as it was 0.58 mm × 89.30 mm × 78.00 mm. The dimensions of the LCP-TF prototype were 0.20 mm × 45.50 mm × 48.30 mm. The silicone sample was 0.60 mm × 78.67 mm × 78.67 mm. The Ad-Tech device was 0.58 mm × 79.65 mm × 80.00 mm. For all iterations of physical measurement, no notable variations were observed with digital calipers (iGaging IP54), which are rated to have a measurement resolution of 0.01 mm and 0.03 mm repeatability.

The forces measured during the four-point flexural bending experiment are presented in table 1. These forces represent the samples physical resistance to a possible flexion of 5 mm. Meaning, the displacement and force required to cause the flexion were generated by the drive nut of the lead screw linear actuator lowering by 5 mm.

The values in table 1, were corrected using the sensor calibration. Both the calibration curves and the raw data for table 1 can be found in the supplementary information. Utilizing Gaussian error propagation, we calculated the errors associated with sample deflection, flexural modulus, and maximum force.
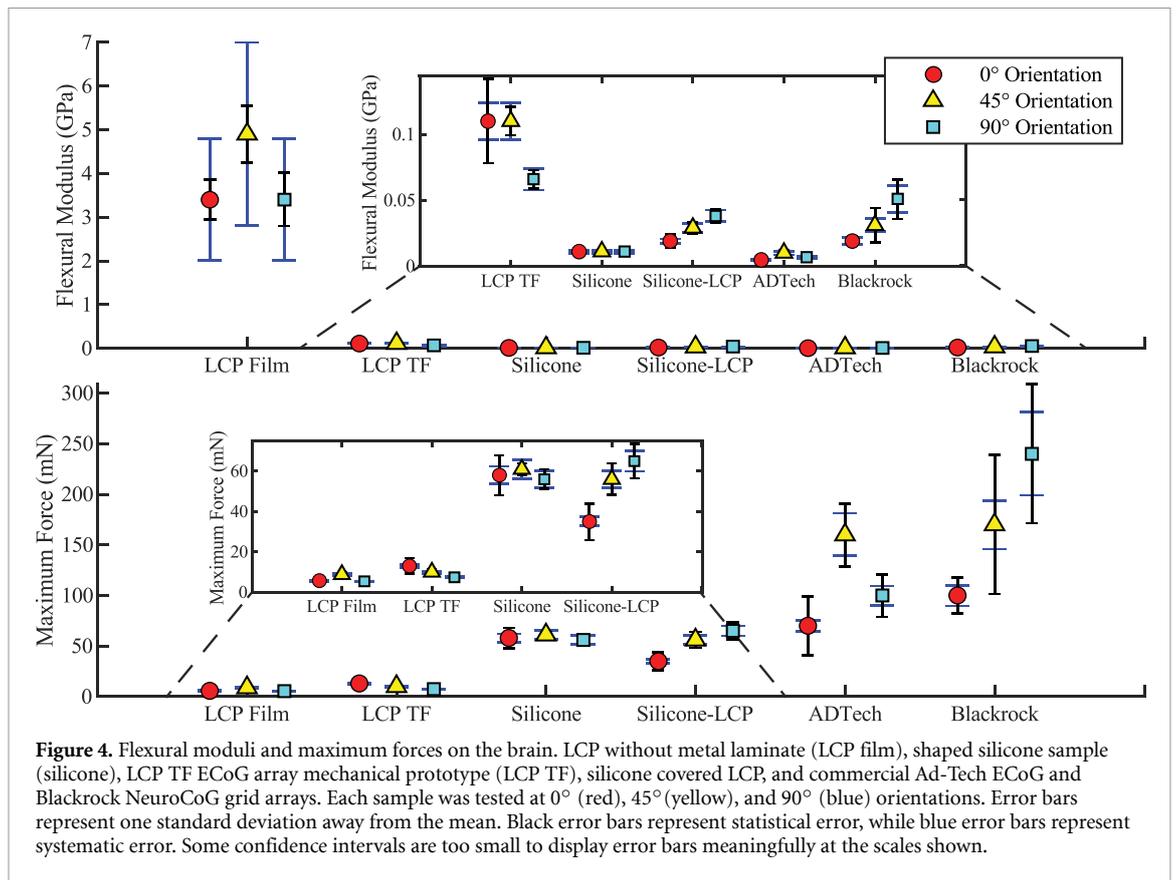
4. Discussion

4.1. Comparing material and mechanical properties
The LCP TF samples and ECoG prototypes demonstrated that they would likely exert 5× to 32× lower force on the brain than the commercially available ECoG arrays tested. The range in this metric depends on which samples and bending directions are being compared (figure 4) despite the LCP film having a larger flexural modulus than the silicone containing samples. The measured flexural modulus on its own is not indicative of the maximum force each sample could exert, as this also depends on the sample geometry.

All materials measured, other than silicone, are known to be linear elastic materials [14, 45–47]. In the supplementary materials, we verified the linearity of similar silicone and LCP TF containing samples with a rheometer (Kinexus Pro+, Netzsch). Additionally, the measured elastic moduli for silicone sheet, LCP film, and CF samples are within the range of literature values for such samples [14, 45–47]. As TF flexural bending is not a standard protocol for non-rigid materials, these measured materials were used in lieu of standard materials to validate the equipment. It was ultimately decided that tensile and compressive tests of these materials would not be able to further test the veracity of the equipment better than our calibration protocol as these tests are known to exhibit different elastic moduli due to anisotropy [34].

4.2. Controlling flexure with orientation and physical patterning
All samples other than silicone seemed to exhibit some level of anisotropy, dependent on bending orientation, in either flexural modulus or maximum

Figure 4. Flexural moduli and maximum forces on the brain. LCP without metal laminate (LCP film), shaped silicone sample (silicone), LCP TF ECoG array mechanical prototype (LCP TF), silicone covered LCP, and commercial Ad-Tech ECoG and Blackrock NeuroCoG grid arrays. Each sample was tested at 0° (red), 45°(yellow), and 90° (blue) orientations. Error bars represent one standard deviation away from the mean. Black error bars represent statistical error, while blue error bars represent systematic error. Some confidence intervals are too small to display error bars meaningfully at the scales shown.
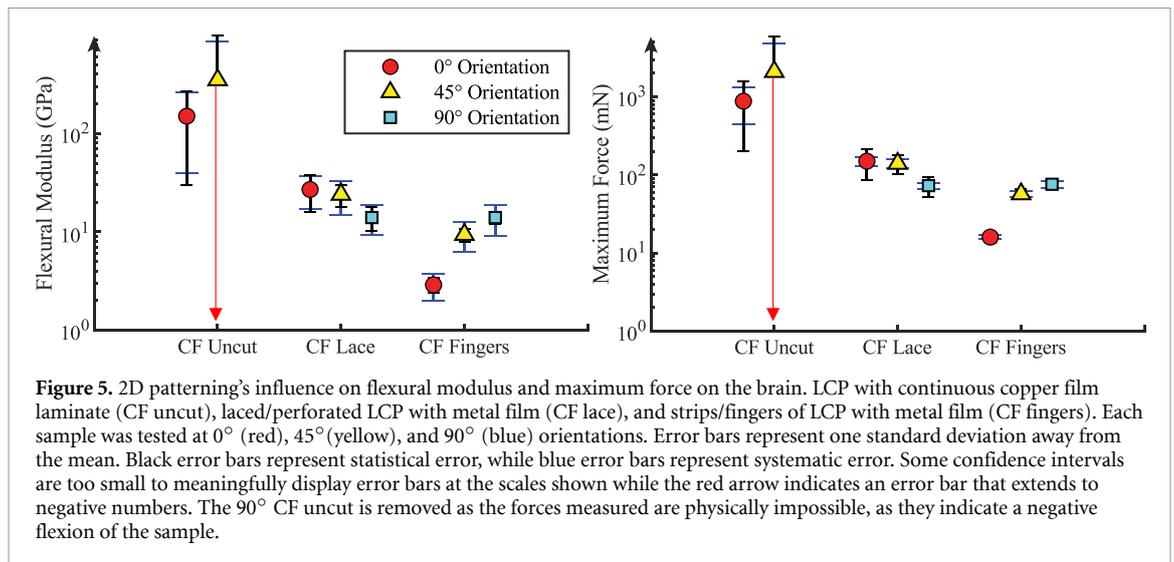
force on the brain. (figure 4). While some samples did not have any wires/fibers that would explain their anisotropy (CF uncut, LCP film, LCP-TF, and silicone-LCP), the measured anisotropy should not be fully discounted as inconsequential as it may have resulted from the test setup (e.g. gravity or friction) or direction dependent tooling (e.g. film drawing/ extrusion direction, tensioned film storage on a spool, or edge effective zone stress hardening during sample patterning.). However, when normalizing for differences in scale, the homogenous samples (LCP film and silicone) did indeed have the lowest levels of anisotropy and the samples with stiff metal wiring (Ad-Tech and Blackrock) had the largest anisotropy.

The flexural modulus and maximum force on the brain were reduced due to the excision of material from the CF samples (figure 5). The large force measured for 45° CF uncut indicates miniscule flexion of the sample, so the error is very large. Flexural anisotropy was modulated based on pattern chosen. The 0° and 45° orientations of the CF fingers were lower than their CF lace counterparts for both flexural modulus and maximum force, while the 90° orientations overlapped. The CF lace and CF fingers both exhibited significantly lower flexural moduli and maximum forces than the 0° CF uncut. This indicates that the rigid portions of an ECoG can be patterned to not only reduce cortical forces and effective flexural moduli

but to also create anisotropy that maintains array stiffness in a chosen direction to assist with its positioning during implantation. It is important to note that decreasing an ECoG array's stiffness to increase its safety *in vivo* by reducing the force exerted on the brain could decrease the ease of use in surgical practice due to making the positioning more difficult. Such trade-offs need to be considered when designing corresponding ECoG devices and finding the optimal working point for these two parameters will need to be explored in future experiments. However, patterning the LCP-TF material offers an efficient way of modifying the rigidity of the device and its anisotropy and thus can support such studies.

It was unexpected that the Ad-Tech and Blackrock samples exhibited strongly different flexure forces for different orientations, as most of their volume consists of silicone. As such an anisotropy is not found in the simple silicone sample, an explanation could be given by the embedded wires and their orientation within the device. This explanation is further supported by the Blackrock array having the lowest bending force in the 0° orientation, in which the wires are bent the least. However, other explanations are equally possible as an anisotropy could also be created during potting/pouring of the silicone as it could cure, cross-link, crystalize, and oxidize at different rates.

Figure 5. 2D patterning's influence on flexural modulus and maximum force on the brain. LCP with continuous copper film laminate (CF uncut), laced/perforated LCP with metal film (CF lace), and strips/fingers of LCP with metal film (CF fingers). Each sample was tested at 0° (red), 45° (yellow), and 90° (blue) orientations. Error bars represent one standard deviation away from the mean. Black error bars represent statistical error, while blue error bars represent systematic error. Some confidence intervals are too small to meaningfully display error bars at the scales shown while the red arrow indicates an error bar that extends to negative numbers. The 90° CF uncut is removed as the forces measured are physically impossible, as they indicate a negative flexion of the sample.

4.3. Verification of testing setup

The data presented above (figure 4) indicates that our testing assembly can perform flexural bending tests on highly flexible ECoG arrays with a high degree of accuracy and repeatability. Despite the sensor's output being lower than hypothesized, post-test calibration allowed for data correction with limited error. This corrected data is presented in table 1 and figures 4 and 5. To improve the resolution of future results, the gain of the instrumentation amplifier could be increased, and a digital position measurement system could be added.

We have shown that while our machine may be comparatively simple, low cost and easy to build, it is able to generate repeatable and accurate data that has predictive power regarding ECoG flexural modulus and the forces it exerts. By using mechanical characterization equipment designed for highly compliant materials, future work can be done to improve this method's ease of use and accuracy.

4.4. Maximum force exerted by experimental ECoG array

Our calculations indicate that the maximum forces exerted on the brain by the prototype LCP-TF grid should be less than 20% of those produced by any FDA-cleared ECoG array tested herein. Unfortunately, the pressure created by this force is largely dependent on the area of contact and how these forces would be distributed. This local pressure determination would require additional material properties to be gathered and for a patient specific finite element model to be generated.

Adding LCP film does increase a composite's elastic modulus; however, its thinner profile and dynamic patterning allow for significantly reduced forces exerted on the brain compared to commercially available ECoG arrays such as those currently made by Ad-Tech and Blackrock. This novel TF production method may enable high-density ECoG arrays to be

chronically implanted, which will open possibilities of their use in brain computer interfaces and as long term neuroprosthetic devices.

The possible non-linearity of our samples should be addressed, as it could be a source of error in estimating maximum bending force. However, our test method was designed to bend the sample near to the point of maximum flexion to mitigate any of these effects. That is in addition to all materials tested linearly increasing in force during deflection and no samples exhibited permanent deformation when removed from the machine [14, 45–47]. Therefore, the maximum bending force is a demonstrably high accuracy interpolative calculation for the lower stiffness samples tested.

While these bending forces are the first step in predicting an ECoG array's impact on the brain, the actual pressures they would manifest and thus physiological effects they would cause cannot be estimated with force information alone due to the complexity of the problem. First, effects that are correlated with mechanical pressure on the brain require knowledge of both applied force and contact area. Besides the bending forces of the array this requires, and exact determination of the contact area and additionally the compression of the brain caused by the thickness of the ECoG array. However, the results of this analysis could vary significantly between patients and on the placement of the ECoG arrays for three reasons:

(a) The skull does not have a uniform radius of curvature and the gyri of the brain cause an uneven morphology (figure S3 in supplementary materials).

(b) The mechanical behavior of the brain is not homogeneous and has non-linear and transient properties related to its fluid mechanics [48–51].

(c) The composition and morphology of the brain changes from person to person [48–51].

Therefore, this study focuses on maximum bending force of the ECoG arrays as it is a metric that is a major factor that can induce a local pressure on the brain and thus should directly correspond to the level of physiological effects caused by the implantation of an ECoG array relative to other ECoG arrays.

Please note that the presented data is only valid for short term application of the devices. For chronic application, the *in vivo* environment (ion containing fluids, foreign body response) can alter the material properties of the device over time [52]. Oxidation and hydrolysis are factors that can accelerate the degradation of polymers [52]. Additionally, body temperature and water absorption can both make the polymeric materials more flexible *in vivo* (compared to the presented dry and room-temperature data) [14, 15, 31]. While LCP is known to be resistive to these kinds of influences, an understanding of the *in vivo* aging of the presented devices will need to be the subject of future studies [31, 50, 51].

Furthermore, a full assessment of the pressure locally exerted on the brain by an ECoG array, will require a detailed study including finite element analysis (FEA) that accounts for populational variations in brain morphology and composition. This analysis will also have to account for variations in surgical practice for common ECoG implantation procedures. Additionally, an *in vivo* study will then be necessary to test the predictions of the FEA with the assistance of medical imaging techniques and force transducers. Such studies could, in the future, allow for the derivation of a generalized relationship between an ECoG array's maximum bending force, its geometry and composition and the mechanical stress it will exert on the brain.

5. Conclusion

With existing flexible circuit manufacturing methods, we created an ECoG array that would exert much lower forces on the brain than commercially available ECoG arrays. To quantify this, we used readily available components to create a low-force, quasistatic materials testing machine that could perform four-point flexural bending tests on ECoG array samples. The outcome of the mechanical testing confirmed that: (a) the custom-made materials testing machine had sufficient capabilities to characterize thin flexible samples; (b) the developed LCP-TF prototype device will exert lower forces on the brain than existing silicone grid devices by Ad-Tech or Blackrock (c) Variations of thickness, implementation of finger structures or strips of LCP, and laced/perforated films allow us to tune the flexible properties as well as the isotropy of the mechanical properties with a broad enough parameter space to meet surgeons' needs. This information can be used to inform future ECoG array design choices regarding device stiffness. It can also be used to improve the preclinical testing protocols currently used to evaluate ECoG safety and efficacy. With both advances, ECoG array implant efficacy can be potentially improved to decrease acute and chronic side effects, which are positively associated with ECoG array stiffness.

Contributions

F S conceptualized and supervised the mechanical testing. N W designed and assembled the mechanical testing setup; N W, C R, and T O aided with the data analysis and experimentation; J V, K B, C W, and C C designed and created the LCP-TF electrode prototype; and B P, S D, D F, and F S provided clinical and industry insight for the prototype design. N W wrote the manuscript draft with input and guidance from C R and F S. All authors edited and commented on the manuscript.

ORCID iDs

Nicholas S Witham ⬦ https://orcid.org/0000-0002-6469-4991

Christopher F Reiche ● https://orcid.org/0000-0001-6216-5888

Thomas Odell ● https://orcid.org/0000-0002-0865-8929

Katrina Barth ● https://orcid.org/0000-0002-0193-5057

Chia-Han Chiang ● https://orcid.org/0000-0002-4010-1266

Charles Wang ● https://orcid.org/0000-0002-2283-0529

Sasha Devore ● https://orcid.org/0000-0003-2554-1850

Daniel Friedman ● https://orcid.org/0000-0003-1068-1797

Bijan Pesaran ● https://orcid.org/0000-0003-4116-0038

Jonathan Viventi ● https://orcid.org/0000-0001-6054-0541

Florian Solzbacher ● https://orcid.org/0000-0002-8309-9610

References

[1] Schalk G and Leuthardt E C 2011 Brain-computer interfaces using electrocorticographic signals *IEEE Rev. Biomed. Eng.* **4** 140–54

[2] Leuthardt E C, Schalk G, Wolpaw J R, Ojemann J G and Moran D W 2004 A brain-computer interface using electrocorticographic signals in humans *J. Neural Eng.* **1** 63–71

[3] Henle C, Raab M, Cordeiro J G, Doostkam S, Schulze-Bonhage A, Stieglitz T and Rickert J 2011 First long term *in vivo* study on subdurally implanted micro-ECoG electrodes, manufactured with a novel laser technology *Biomed. Microdevices* **13** 59–68

[4] Leuthardt E C, Schalk G, Roland J, Rouse A and Moran D W 2009 Evolution of brain-computer interfaces: going beyond classic motor physiology *Neurosurg. Focus* **27** 1–11

[5] Pesaran B, Vinck M, Einevoll G T, Sirota A, Fries P, Siegel M, Truccolo W, Schroeder C E and Srinivasan R 2018 Investigating large-scale brain dynamics using field potential recordings: analysis and interpretation *Nat. Neurosci.* **21** 903–19

[6] Cogan G B, Thesen T, Carlson C, Doyle W, Devinsky O and Pesaran B 2014 Sensory–motor transformations for speech occur bilaterally *Nature* **507** 94–98

[7] Cogan G B, Iyer A, Melloni L, Thesen T, Friedman D, Doyle W, Devinsky O and Pesaran B 2017 Manipulating stored phonological input during verbal working memory *Nat. Neurosci.* **20** 279–86

[8] Chang E F 2015 Towards large-scale, human-based, mesoscopic neurotechnologies *Neuron* **86** 68–78

[9] Dubey A and Ray S 2019 Cortical electrocorticogram (ECoG) is a local signal *J. Neurosci.* **39** 4299–311

[10] Abhinav K, Prakash S and Sandeman D R 2013 Use of robot-guided stereotactic placement of intracerebral electrodes for investigation of focal epilepsy: initial experience in the UK *Br. J. Neurosurg.* **27** 704–5

[11] Voorhies J and Cohen-Gadol A 2013 Techniques for placement of grid and strip electrodes for intracranial epilepsy surgery monitoring: pearls and pitfalls *Surg. Neurol. Int.* **4** 98

[12] Yeager J D, Phillips D J, Rector D M and Bahr D F 2008 Characterization of flexible ECoG electrode arrays for chronic recording in awake rats *J. Neurosci. Methods* **173** 279–85

[13] Kohler F, Michiels R, Schuettler M and Stieglitz T 2015 Development of a bending test procedure for the characterization of flexible ECoG electrode arrays *Curr. Dir. Biomed. Eng.* **1** 510–4

[14] Fekete Z and Pongrácz A 2017 Multifunctional soft implants to monitor and control neural activity in the central and peripheral nervous system: a review *Sens. Actuators* B **243** 1214–23

[15] Schendel A A, Eliceiri K W and Williams J C 2014 Advanced materials for neural surface electrodes *Curr. Opin. Solid State Mater. Sci.* **18** 301–7

[16] Woods V, Trumpis M, Bent B, Palopoli-Trojani K, Chiang C-H, Wang C, Yu C, Insanally M, Froemke R C and Viventi J 2018 Long-term recording reliability of liquid crystal polymer μECoG arrays *J. Neural Eng.* **15** 066024

[17] Blackmore J, Shrivastava S, Sallet J, Butler C R and Cleveland R O 2019 Ultrasound neuromodulation: a review of results, mechanisms and safety *Ultrasound Med. Biol.* **45** 1509–36

[18] Wahab R A, Choi M, Liu Y, Krauthamer V, Zderic V and Myers M R 2012 Mechanical bioeffects of pulsed high intensity focused ultrasound on a simple neural model *Med. Phys.* **39** 4274–83

[19] Bjornsson C S, Oh S J, Al-Kofahi Y A, Lim Y J, Smith K L, Turner J N, De S, Roysam B, Shain W and Kim S J 2006 Effects of insertion conditions on tissue strain and vascular damage during neuroprosthetic device insertion *J. Neural. Eng.* **3** 196–207

[20] Wan W H, Ang B T and Wang E 2008 The Cushing response: a case for a review of its role as a physiological reflex *J. Clin. Neurosci.* **15** 223–8

[21] Fong J S, Alexopoulos A V, Bingaman W E, Gonzalez-Martinez J and Prayson R A 2012 Pathologic findings associated with invasive EEG monitoring for medically intractable epilepsy *Am. J. Clin. Pathol.* **138** 506–10

[22] Tandon N, Tong B A, Friedman E R, Johnson J A, Von Allmen G, Thomas M S, Hope O A, Kalamangalam G P, Slater J D and Thompson S A 2019 Analysis of morbidity and outcomes associated with use of subdural grids vs stereoelectroencephalography in patients with intractable epilepsy *JAMA Neurol.* **76** 672–81

[23] Albert G W, Dahdaleh N S, Reddy C, Hansen D R, Vogel T W, Kawasaki H and Howard M A 2010 Postoperative radiographic findings in patients undergoing intracranial electrode monitoring for medically refractory epilepsy: clinical article *J. Neurosurg.* **112** 449–54

[24] Moshayedi P, Ng G, Kwok J C F, Yeo G S H, Bryant C E, Fawcett J W, Franze K and Guck J 2014 The relationship between glial cell mechanosensitivity and foreign body reactions in the central nervous system *Biomaterials* **35** 3919–25

[25] Hong G and Lieber C M 2019 Novel electrode technologies for neural recordings *Nat. Rev. Neurosci.* **20** 330–45

[26] Chen R, Canales A and Anikeeva P 2017 Neural recording and modulation technologies *Nat. Rev. Mater.* **2** 16093

[27] Teo A J T, Mishra A, Park I, Kim Y J, Park W T and Yoon Y J 2016 Polymeric biomaterials for medical implants and devices *ACS Biomater. Sci. Eng.* **2** 454–72

[28] DYCONEX AG 2010 DYCONEX's liquid crystal polymer (LCP) substrate proves cytotoxicity conformity according to ISO 10993–5

[29] Schulze D, Tolke R and Widmann I 2014 Noble metal PCB manufacturing for direct implants *PCB Magazine*

[30] Chiang C *et al* 2021 Flexible, high-resolution thin-film electrodes for human and animal neural research *J. Neural Eng.* **18** 045009

[31] Jeong J, Bae S H, Seo J-M, Chung H and Kim S J 2016 Long-term evaluation of a liquid crystal polymer (LCP)-based retinal prosthesis *J. Neural. Eng.* **13** 025004

[32] Liu D S and Chao Y C 2003 Effects of dopant, temperature, and strain rate on the mechanical properties of micrometer gold-bonding wire *J. Electron. Mater.* **32** 159–65

[33] Chung S M, Yap A U J, Chandra S P and Lim C T 2004 Flexural strength of dental composite restoratives: comparison of biaxial and three-point bending test *J Biomed. Mater. Res.* B **71** 278–83

[34] Mujika F 2006 On the difference between flexural moduli obtained by three-point and four-point bending tests *Polym. Test.* **25** 214–20

[35] Junior S A R, Ferracane J L and Della Bona Á 2008 Flexural strength and Weibull analysis of a microhybrid and a nanofill composite evaluated by 3- and 4-point bending tests *Dent. Mater.* **24** 426–31

[36] Blackrock Neurotech 2018 Electrode concepts Blackrock Microsystems (available at: https://blackrockneurotech.com/research/neuroscience-research-products/low-noise-ephys-electrodes/blackrock-electrode-concepts/) (Accessed 16 July 2019)

[37] United States Food Drug Administration (FDA) 2020 K191346: Blackrock NeuroCoG Subdural Cortical Electrodes (Strips and Grids) approval letter (available at: www.accessdata.fda.gov/cdrh_docs/pdf19/K191346.pdf) (Accessed 20 July 2022)

[38] Lesser R P, Crone N E and Webber W R S 2010 Subdural electrodes *Clin. Neurophysiol.* **121** 1376–92

[39] AdTech Product Catalogue Sev. Healthc. Technol. Ltd vol VII (available at: www.severnhealthcare.com/images/documents/ad-tech/AD-TECHCatalogue-2015.pdf) (Accessed 16 July 2019)

[40] 2015 *National Instruments Specifications NI myDAQ* (available at: www.ni.com/docs/en-US/bundle/mydaq-specs/page/specs.html) (Accessed 31 July 2019)

[41] ADInstruments 2010 Model 1030 force transducer instructions 1–8 (available at: www.ufiservingscience.com/model_1030.html) (Accessed 5 October 2010)

[42] Zhu Z, Zhu S, Zhu J, Van der Giet M and Tepel M 2002 Endothelial dysfunction in cold-induced hypertensive rats *Am J. Hypertens* **15** 176–80

[43] Ábrigo J, Simon F, Cabrera D and Cabello-Verrugio C 2016 Angiotensin-(1-7) prevents skeletal muscle atrophy induced by transforming growth factor type beta (TGF-β) via mas receptor activation *Cell Physiol. Biochem.* **40** 27–38

[44] Kugler E M, Michel K, Zeller F, Demir I E, Ceyhan G O, Schemann M and Mazzuoli-Weber G 2015 Mechanical stress activates neurites and somata of myenteric neurons *Front. Cell. Neurosci.* **9** 1–17

[45] ASTM Committee D20 2014 *Standard Test Method for Flexural Properties of Unreinforced and Reinforced Plastics and Electrical Insulating Materials by Four-Point Bending (D 790)* (ASTM International) pp 1–9 (available at: www.astm.org/c1341-13r18.html)

[46] ASTM Committee C-28 2010 *Standard Test Method for Flexural Properties of Continuous Fiber-Reinforced Advanced Ceramic Composites (C 1341 – 00)* (ASTM International) pp 1–11 (available at: www.astm.org/c1341-00.html)

[47] Ku H H 1966 Notes on the use of propagation of error formulas *J. Res. Natl. Bur. Stand.* C *Eng. Instrum.* **70C** 263–73

[48] Walsh E K and Schettini A 2019 Calculation of brain elastic parameters *in vivo Am J. Physiol.* **247** 693–700

[49] Hrapko M, Gervaise H, van Dommelen J A W, Peters G W M and Wisemans J S H M 2007 Identifying the mechanical behaviour of brain tissue *IRCOBI Conf.* pp 143–59

[50] Miller K, Chinzei K, Orssengo G and Bednarz P 2000 Mechanical properties of brain tissue *in-vivo*: experiment and computer simulation *J. Biomech.* **33** 1369–76

[51] Goriely A, Geers M G D, Holzapfel G A, Jayamohan J, Jérusalem A, Sivaloganathan S, Squier W, van Dommelen J A W, Waters S and Kuhl E 2015 Mechanics of the brain: perspectives, challenges, and opportunities *Biomech. Model. Mechanobiol.* **14** 931–65

[52] Hukins D W L, Mahomed A and Kukureka S N 2008 Accelerated aging for testing polymeric biomaterials and medical devices *Med. Eng. Phys.* **30** 1270–4

[53] Hwang G T *et al* 2013 *In vivo* silicon-based flexible radio frequency integrated circuits monolithically encapsulated with biocompatible liquid crystal polymers *ACS Nano* **7** 4545–53